

Mobility of Proteins in Highly Hydrated Polyelectrolyte Multilayer Films

Cédric Vogt,^{†,‡} Vincent Ball,^{†,‡} Jérôme Mutterer,[§] Pierre Schaaf,^{||} Jean-Claude Voegel,^{†,‡} Bernard Senger,^{*,†,‡} and Philippe Laval^{†,‡,⊥}

[†]Institut National de la Santé et de la Recherche Médicale, Unité 977, 11 rue Humann, 67085 Strasbourg Cedex, France

[‡]Faculté de Chirurgie Dentaire, Université de Strasbourg, 1 place de l'Hôpital, 67000 Strasbourg, France

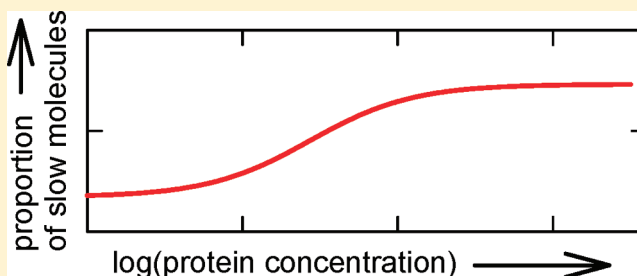
[§]Centre National de la Recherche Scientifique, UPR 2357, Institut de Biologie Moléculaire des Plantes, 12 rue du Général Zimmer, 67084 Strasbourg Cedex, France

^{||}Centre National de la Recherche Scientifique, UPR 22, Institut Charles Sadron, 23 rue du Loess, BP 84047, 67034 Strasbourg Cedex 2, France

[⊥]Hôpitaux Universitaires de Strasbourg, 1 place de l'Hôpital, 67000 Strasbourg, France

S Supporting Information

ABSTRACT: The lateral diffusion of a protein (human serum albumin labeled with fluorescein isothiocyanate) within a highly hydrated polyelectrolyte film is studied. The film is built up with poly(L-lysine) as polycation and hyaluronate as polyanion. Fluorescence recovery after photobleaching is used to evaluate the mobility of the labeled protein. Spatial Fourier transformation is applied to the fluorescence intensity recorded at various times after bleaching of a narrow rectangular area within an image representative of the film. This approach necessitates no hypothesis on the intensity distribution at the end of the bleaching provided that the bleach has not appreciably changed the concentration ratios of the different diffusing species. Furthermore, under the hypothesis that molecules move according to Fick's law, we represent the Fourier transform by a weighted sum of exponentials each containing another diffusion coefficient and evaluate the proportion attached to each term of this sequence using the simulated annealing method. A criterion, combining goodness-of-fit and the entropy characterizing the diffusion coefficient spectrum, is proposed to avoid overinterpretation of the experimental data. The optimum spectrum of the diffusion coefficient is then extracted from the time evolution of the light intensity at various albumin concentrations within the films. It appears that the mobility, quantified by the amount of tracer molecules having a diffusion coefficient smaller than, e.g., $0.1 \mu\text{m}^2/\text{s}$, undergoes a transition between 20 and $2000 \mu\text{g/mL}$ of internal concentration. This suggests that the mutual interactions of the albumin molecules and the interactions between fluorescently labeled albumin and the film network become increasingly important in the reduction of the albumin mobility as the albumin concentration increases.



INTRODUCTION

"Polyelectrolyte multilayers" is a generic term to designate films constructed by the self-assembly of polyanions and polycations via the layer-by-layer (LbL) method.¹ Widespread applications are concerned with LbL ranging from materials science^{2–5} to biology.^{6–8} Two types of polyelectrolyte multilayer films were depicted: those whose thickness and mass increase linearly with the number of deposition steps and those for which this growth is exponential at least at the beginning of their buildup.^{9,10} Lateral mobility of polyelectrolyte chains in linearly growing films has been still recently determined. For example, in the case of PSS/PAH (PSS, poly(sodium 4-styrene sulfonate); PAH, poly(allylamine hydrochloride)) multilayers, the diffusion coefficient of fluorescein isothiocyanate (FITC)-labeled PAH was lower than $10^{-6} \mu\text{m}^2/\text{s}$ which corresponds to a glassy state.^{11,12} It was also shown, using neutron reflectometry, that the mobility of polyelectrolytes in a linearly growing film can be

favorable by an increased salt concentration.¹³ In exponentially growing multilayers, polyelectrolytes display a much higher lateral mobility. PLL/HA films (PLL, poly(L-lysine); HA, hyaluronic acid) are typical films whose thickness increases exponentially with the number of deposition steps at the beginning of the buildup.⁹ The mobility of labeled PLL was investigated by fluorescence recovery after photobleaching (FRAP) where we assumed that the labeled chains were either mobile or immobile, i.e., that there were only two populations.¹⁴ A more sophisticated method, though quite tedious to implement, consisted of producing a pattern of fringes, alternatively bright and dark, and to derive the diffusion coefficients from the time decay of the contrast between the fringes.

Received: January 2, 2012

Revised: March 27, 2012

Published: April 9, 2012

Thus, three PLL populations were identified: one population with a “high” diffusion coefficient ($D \approx 1 \mu\text{m}^2/\text{s}$), another with a smaller diffusion coefficient, and a third population, which was considered as immobile ($D < 0.001 \mu\text{m}^2/\text{s}$).¹⁵

Because exponentially growing multilayers can act as microcontainers (or reservoirs) for active compounds, it is interesting to evaluate the capability of such molecules to diffuse inside them. Now, the film can be loaded at various concentrations depending on the concentration of the solution to which it is exposed as well as on the exposure time.¹⁶ Paclitaxel (Taxol) was incorporated into a PLL/HA stratum at a concentration up to 1 order of magnitude higher than that of the solution brought into contact with the film. Other examples have been published more recently concerning the loading of polyelectrolyte multilayers with biomolecules, as for example TAT peptides,¹⁷ BMP-2 proteins,¹⁸ antimicrobial peptides,¹⁹ vancomycin,²⁰ or a model protein,²¹ for local delivery.

The loading of PLL/HA films with proteins like human serum albumin (HSA) has to our knowledge not been studied. HSA, a protein of 66 kDa with an isoelectric point of 4.7, makes up about 55% of the total human blood proteins.²² Diffusion of HSA adsorbed “on” or embedded “in” polyelectrolyte multilayers has been described only for linearly growing, thin polyelectrolyte multilayers, namely PSS/PAH films.^{23,24} In the present article, we propose to study the loading and the mobility of this model protein in PLL/HA films. Indeed, it may be hypothesized that the mobility of the loaded molecules is sensitive to their concentration and to the polymeric environment, notably when free positively charged PLL chains (polycations), or PLL chains whose charges are extrinsically compensated to some extent, are available for complexation with negatively charged proteins, such as albumin which wears 5 binding sites for cationic species.²⁵ First, we will check that HSA labeled with fluorescein isothiocyanate (HSA^{FITC}) can be loaded in thick PLL/HA films with a resulting homogeneous distribution in the film section. The loading rates will be evaluated as a function of the solution concentration brought into contact with the films for a fixed time.

Then, FRAP experiments will be performed using HSA^{FITC} . The confocal microscopy images will be processed following a method based on spatial Fourier analysis applied to images where a rectangular area was bleached.^{26,27} An alternative would consist in bleaching a circular area and using the Hankel transform.²⁸ In both cases, the goal of the processing is to determine the diffusion coefficient of the labeled molecule or, better, its distribution over a large interval avoiding any hypothesis on the number of components, i.e., of populations differing by their diffusion coefficient. A quantity of prime significance in the method presented here is the entropy associated to this distribution, the so-called Shannon-Jaynes entropy.^{29–32} The weight of each diffusion coefficient within a sequence of possible values given a priori is determined using the algorithm called “simulated annealing”,^{33,34} which was not used previously in this context to our knowledge. As this procedure goes on, the agreement between the simulated and experimental data improves and the distribution structures, i.e., the entropy gradually decreases. This is synonymous with gain of information. However, the reduction of entropy becomes meaningless once the improvement of fit quality becomes small. Then, the procedure is stopped. This strategy, concisely outlined, relies on the “principle of minimum information”³⁵ or “principle of parsimony”³⁶ which states that the fitting procedure should not add information which is not warranted by the experimental measurements (see also ref 37).

This procedure allows determining the distribution of the lateral diffusion coefficient of the labeled protein in the PLL/HA films for various protein concentrations within the film. It will reveal a concentration interval over which the proportion of slowly moving HSA^{FITC} molecules increases substantially. This reduction of mobility likely mirrors the effect of an increasingly crowded medium and of the interaction of the labeled molecules with themselves and with their polymeric environment. The role of crowding and binding has been recently evidenced even in solution.³⁸

MATERIALS AND METHODS

Preparation of Polyelectrolyte Films. Poly(L-lysine) hydrobromide (PLL, 60 kDa, Sigma-Aldrich, Saint Quentin Fallavier, France) and sodium hyaluronate (HA, 400 kDa, Lifecore Biomedical, Chaska, U.S.A.) were used to build up $(\text{PLL/HA})_n$ -PLL films, where n stands for the number of pairs of polyelectrolytes deposited; it is fixed to 24 in the present study. Polyelectrolyte solutions were prepared by dissolution of the respective adequate polymer amounts in a 0.15 M NaCl aqueous solution buffered at pH 7.4 with 10 mM tris(hydroxymethyl)aminomethane (TRIS). All solutions were prepared using ultrapure water (resistivity close to $18.2 \text{ M}\Omega\cdot\text{cm}$). 12-mm glass slides (Marienfeld GmbH & Co.KG, Lauda-Königshofen, Germany) were used as substrates and were cleaned before use with a 70% v/v ethanol solution, a 2% v/v Hellmanex solution and a 0.1 M HCl solution (each cleaning step was followed by a rinsing step with water, each lasting 15 min). The films were constructed with an automatic machine (Dipping Robot DR3, Riegler & Kirstein GmbH, Potsdam, Germany) by repeating the following sequences where the glass slides are dipped in (i) a polycation bath (8 min), (ii) two rinsing solutions ($2 \times 5 \text{ min}$), (iii) a polyanion bath (8 min), and then (iv) two rinsing solutions ($2 \times 5 \text{ min}$). Then, the films were stored in a TRIS-buffered 0.15 M NaCl solution at 4 °C.

Loading of Films. The loading capacity of the $(\text{PLL-HA})_{24}$ -PLL films was evaluated for HSA^{FITC} (with 10 mols of FITC per mole of HSA, Sigma-Aldrich, Schnellendorf, Germany). To this end, 500 μL of protein solution at a defined concentration were deposited on top of the film and the solution stayed for 30 min before rinsing with $3 \times 1 \text{ mL}$ of pure buffer ($3 \times 10 \text{ min}$). Then, either for the evaluation of the protein uptake or for the FRAP experiments, the loaded films were examined after a waiting time of about 22 h at room temperature.

Determination of Loading Rates. UV spectroscopy was used to determine the amount of proteins taken up by the films for a given concentration of the solution during contact. This method allows determining the concentration within the loaded film according to its UV absorption at the wavelength 495 nm. For conversion of absorption into concentration, a calibration curve based on UV absorption of solutions of HSA^{FITC} of different known concentrations was established.

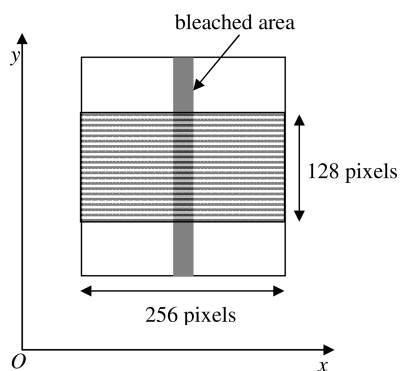
Confocal Laser Scanning Microscopy (CLSM). The bleaching and imaging of films loaded with HSA^{FITC} were performed on a Zeiss LSM 510 confocal microscope equipped with an argon laser (488 nm). During observation, the slides coated with the films were placed in a homemade sample holder filled with 1 mL of TRIS-buffered 0.15 M NaCl solution, in order to avoid drying of the film. A 10 \times objective lens with a numerical aperture of 0.3 (Zeiss Plan Neofluar) was used. The numerical zoom was fixed to $\times 3$ in order to define a $300 \times 300 \mu\text{m}^2$ image ($L = 300 \mu\text{m}$). The area of an image was virtually subdivided into $N \times N = 256 \text{ pixels} \times 256 \text{ pixels}$.

z-sections of the films were also obtained after deconvolution and reconstruction of (x, y) stacked images.

FRAP Protocol. First, a prebleach image of the sample was recorded. Then, typical bleaching consisted in scanning 500–2000 times a 256 pixels \times 10 pixels or a 256 pixels \times 20 pixels rectangle in the prebleach image drawn by using the bleaching tool of the software (Carl Zeiss AIM 510 version 3.2). This area was bleached with the laser set at its maximum power. The 10 \times objective used for photobleaching yields optical sections that are thicker than the film thickness itself: from 11 μm up to more than 50 μm , depending on the value of the pinhole diameter used. Consequently, the film was bleached over its whole thickness during this procedure. The bleach time was adjusted to achieve sufficient contrast between the bleached and nonbleached regions. After the bleach, images were acquired at times ranging from ca. 10 s up to ca. 1000 s to monitor the recovery process. These images were acquired by scanning the sample with the laser power carefully chosen to have an acceptable signal-to-noise ratio while avoiding strong bleach during image acquisition (“reading” step).

Image Processing. The images were analyzed by means of a macro executed with the software “Image J” (Rasband, W. S., ImageJ, U.S. National Institutes of Health, Bethesda, Maryland, U.S.A., <http://imagej.nih.gov/ij/>, 1997–2011). In each image, i.e., at each postbleach time, the intensity was recorded on $N \times N = 65536$ pixels. However, only those constituting the $N/2 = 128$ central lines, each 1-pixel wide and perpendicular to the long edges of the bleached zone, i.e., parallel to the Ox axis (Scheme 1), were processed (see below “Power Spectral

Scheme 1. Schematic View of a Square Image Containing a Partially Bleached Rectangle (10 or 20 Pixels Wide; Grey)^a



^aEven immediately after the bleach, the contour of the rectangle is generally not as sharp as suggested in the scheme, due to diffusion of the labeled molecules already during the bleach time (so-called “corona effect”^{39,40}). The processed region consisting of the $N/2 = 128$ central lines of the image, parallel to the Ox axis, is shown.

Density Derived from a Discretized Image”). The two rectangular margins each 64-pixel wide in the Oy direction were left out to avoid border effects due to the diffusion of labeled molecules through the short edges of the bleached rectangle.

COMPUTATIONAL BACKGROUND

Fick’s Law and Spatial Fourier Transform. The starting point of the experimental data analysis is the classical diffusion equation (also called Fick’s law). Note that doing so implicitly assumes that the fluorescent molecule experiences no

anomalous diffusion^{41,42} and that no flux will contribute a systematic component to its movement (diffusion-convection model⁴³). Then, in a one-dimensional Brownian diffusion process (along the Ox axis in Scheme 1, assuming that there is no concentration gradient along the Oy axis in the central zone), the molecule concentration $c(x, t)$ at point x and time t evolves according to

$$\frac{\partial c(x, t)}{\partial t} = D \frac{\partial^2 c(x, t)}{\partial x^2} \quad (1)$$

where D is the diffusion coefficient. Applying the spatial Fourier transformation to eq 1 leads to

$$\frac{\partial C(q, t)}{\partial t} = -q^2 D C(q, t) \quad (2)$$

where $C(q, t)$ is the complex spatial Fourier transform of $c(x, t)$, corresponding to the spatial angular frequency q . The resolution of the ordinary differential equation (eq 2) leads to

$$C(q, t) = C(q, 0) e^{-q^2 D t} \quad (3)$$

The power spectral density (PSD) is defined as the squared modulus of the Fourier transform, i.e., $\text{PSD}(q, t) = |C(q, t)|^2$. As a consequence of eq 3, if all labeled molecules diffused with the same diffusion coefficient D , $\text{PSD}(q, t)$ would decay exponentially with time²⁷ according to

$$\text{PSD}(q, t) = \text{PSD}(q, 0) e^{-2q^2 D t} \quad (4)$$

where $\text{PSD}(q, 0)$ is a unknown proportionality factor.²⁶ Equation 4 is exact whatever the concentration profile at the end of the bleach.^{26,44} In other words, the diffusion which occurs during the bleach process has no importance in the special case where all labeled molecules are moving and have the same diffusion coefficient as in ref 27.

Power Spectral Density Derived from a Discretized Image. Now, consider the light intensity recorded along one of the $N/2 = 128$ lines parallel to the Ox axis, located in the striped region in Scheme 1. This signal, assumed proportional to the concentration of labeled molecules, is known in a sequence of N discrete locations, i.e., the N pixels introduced above ($0 \leq n \leq N - 1$). Then, the Fourier transform of this discretized signal, $s(n, t, l)$, must be computed as a discrete Fourier transform (DFT) defined by

$$S(k, t, l) = \sum_{n=0}^{N-1} s(n, t, l) e^{-i2\pi kn/N} \quad (5)$$

where l means the number of the line and $N/4 \leq l \leq 3N/4 - 1$ according to Scheme 1 (the lines are numbered from 0 up to $N - 1$). The harmonics number, k , is an integer and the spatial frequency introduced above is related to k by $q = (2\pi k/L)$ (radian/ μm) for an image of side length L . The experimental power spectral density (PSD_{exp}) is defined as the squared modulus of the Fourier transform, i.e., $\text{PSD}_{\text{exp}}(k, t, l) = |S(k, t, l)|^2$. It can be noted that $|S(N - k, t, l)|^2 = |S(k, t, l)|^2$. Therefore, for a signal measured on N pixels, the PSD_{exp} corresponding to $N/2 \leq k \leq N - 1$ are redundant with the PSD_{exp} corresponding to $1 \leq k \leq N/2$. Furthermore, because an experimental signal is ever noisy, only the first few harmonics are taken into account.²⁶

Diffusion Coefficient Distribution. In general, several populations of labeled molecules may be present in the film. We assume that they are chemically identical, have the same

light emission, but differ by their mobility. The diffusion coefficient characteristic of each group and even the number of groups are usually unknown. Then, assuming only that the sought diffusion coefficients are located between D_1 and D_m , eq 4, generalizes to

$$\text{PSD}(k, t) = \text{PSD}(k, 0) \left(\sum_{j=1}^m p_j e^{-\left(\frac{2\pi k}{L}\right)^2 D_j t} \right)^2 \quad (6)$$

in the case of 1D-diffusion in the direction parallel to image side of length L perpendicular to the bleached stripe. Here, p_j (≥ 0 and ≤ 1) represents the proportion of the j th component of the spectrum and $\sum_{j=1}^m p_j = 1$. It may be stressed that molecules do already diffuse during the bleaching step.^{39,40} Then, if there are two or more populations of fluorescent molecules, the bleach will penalize the molecules according to their mobility: the more mobile a molecule is, the more underestimated will appear its relative abundance. In general, the accuracy of eq 6 is not as high as that of eq 4. It is therefore important to reduce the bleach time as much as possible. The diffusion coefficients D_j in eq 6 represent the abscissas of the discrete diffusion coefficient spectrum. They constitute a geometric sequence; that is, they are equally spaced on a logarithmic scale as is commonly done for the spectra of the diffusion coefficient³² or of the decay time of fluorescence.^{30,37,45}

Fitting Procedure. Equation 6 must be fitted to the experimental PSD values (PSD_{exp}) derived from the recorded intensities using relation 5. Note that only a relatively small number of harmonics are relevant because of the growing contamination of the PSD_{exp} by the experimental noise as k increases.²⁶ In the cases that will be shown below, we used $k = 1, 2$, and 3 .

The goodness-of-fit is defined using $\langle \text{PSD}_{\text{exp}}(k, t) \rangle$, the average of the $\text{PSD}_{\text{exp}}(k, t)$ corresponding to each of the $N/2 = 128$ central lines evoked above for a given harmonics and a given image (or postbleach time) and the corresponding standard error, $\text{SE}_{\text{exp}}(k, t)$

$$\epsilon^2 = \sum_k \sum_t \left(\frac{\text{PSD}(k, t) - \langle \text{PSD}_{\text{exp}}(k, t) \rangle}{\text{SE}_{\text{exp}}(k, t)} \right)^2 \quad (7)$$

where $\text{PSD}(k, t)$ is defined by eq 6.

In the present work, the possible diffusion coefficients are distributed over the interval $10^{-3} - 10^3 \mu\text{m}^2/\text{s}$. Choosing $m = 60$ leads to $D_{j+1} = D_j \times 10^{0.1}$ and $D_1 = 10^{-2.95} \mu\text{m}^2/\text{s}$. The proportions p_j are fixed to $1/m$ at the beginning of the fitting procedure. This initially flat spectrum corresponds to the maximum entropy $S_{\text{max}} = \ln m$, i.e., to the least information. Then, the p_j are optimized using an algorithm called “simulated annealing”.^{33,34} Because this method relies strongly on the Metropolis algorithm widely used in statistical mechanics,⁴⁶ we must introduce a control parameter which plays the role of the temperature in statistical mechanics. It is usually written T to underscore the analogy and is called “temperature”. In fact, it should be called “thermal energy” because it replaces kT rather than T . The “system” is then slowly “cooled”. At each temperature stage, 5×10^4 sequences are generated. A sequence is obtained from the former by an elementary random change of each p_j defined by

$$\Delta p_j = \frac{0.1}{m} (2u - 1) \quad (8)$$

where u is a random number uniformly distributed over $[0, 1]$, produced using the function “drand” available in the Fortran software (Compaq Visual Fortran, Professional Edition Version 6.5). It may be underscored that in eq 6, the bounds D_1 and D_m are arbitrarily small and large, respectively. However, some attention must be paid to D_m . Indeed, for a large diffusion coefficient, the corresponding exponential in eq 6 becomes extremely small even for $k = 1$ and the smallest time, t_1 . Therefore, in the new sequence of p_j , one of the proportions, chosen at random with the probability equal to $1 - e^{-(2\pi/L)^2 D_j t_1}$, is tentatively turned to zero to avoid the appearance of poorly controlled components in the spectrum that may occur in its high- D wing. With this new sequence of p_j , $\text{PSD}(k, t)$ is computed to evaluate ϵ^2 according to eq 7. The new sequence of p_j is accepted if its associated ϵ^2 ($= \epsilon_{\text{new}}^2$) is smaller than the ϵ^2 value of the previous accepted (“old”) sequence ($= \epsilon_{\text{old}}^2$). If it is larger, it is accepted with the probability defined by

$$P_{\text{acc}} = \exp \left(- \frac{\epsilon_{\text{new}}^2 - \epsilon_{\text{old}}^2}{T} \right) \quad (9)$$

If acceptance fails, the “old”, i.e., former, stored sequence replaces the new, rejected one. Therefore, it happens that a given sequence appears several times in accordance with the principle of the Metropolis algorithm aimed at simulating equilibrium configurations. Once the 5×10^4 sequences are produced, the mean sequence, $\langle p_j \rangle_T$, $j = 1, \dots, m$ is recorded, as well as the associated $\epsilon^2(T)$ and entropy $S(T)$ defined by²⁹

$$S(T) = - \sum_{j=1}^m \langle p_j \rangle_T \ln \langle p_j \rangle_T \quad (10)$$

Then, the temperature is reduced by a factor of 0.9 and again 5×10^4 sequences are generated. This procedure goes on until the system becomes so cold that most attempts to change the sequence of p_j are rejected. We fix this rejection rate to 0.99. The cooling process stops when the rejection rate exceeds 0.99 for ten successive temperatures.

At this stage, the agreement can practically no further improve and the entropy has decreased compared to its initial value $\ln m$. However, already at a temperature generally well above the final temperature, it can be observed that ϵ^2 is near its final value. In contrast, S still decreases visibly. This means that the gain of information, i.e., the structuring of the spectrum, is illusory. This means also that, when completed, the cooling procedure reaches too low a temperature and that a more “reasonable” temperature must be sought. To this end, we suggested to build a function of T , $\delta(T)$, defined by

$$\delta(T) = a(T) - b(T) \quad (11a)$$

where

$$a(T) = \frac{\epsilon_{\text{max}}^2 - \epsilon^2(T)}{\epsilon_{\text{max}}^2 - \epsilon_{\text{min}}^2}$$

$$b(T) = \frac{S_{\text{max}} - S(T)}{S_{\text{max}} - S_{\text{min}}} \quad (11b)$$

As can be seen, $a(T)$ is linked to the evolution of the goodness-of-fit with T . Similarly, $b(T)$ represents the evolution with T of the information provided by the diffusion coefficient spectrum. As will be seen on the examples (Figures 4–6), $\delta(T)$ passes through a maximum located at the temperature T_0 . We use this

temperature as the optimum one. This means that below T_0 the reduction of ϵ^2 is too weak to validate the corresponding reduction of S or gain of information. Clearly, this method of optimum temperature choice is somewhat arbitrary but has the advantage of being independent of the experimentalist's appreciation. It is especially worth noting that this method may be considered as a maximum entropy method (MEM) because T_0 is chosen so that the fit of the calculated PSD to the experimental PSD is obtained without undue reduction of S . The system is then warmed up from the final temperature up to the optimum one (T_0) and 2×10^6 sequences of p_j are generated. Acceptance/rejection of a sequence follows the same Metropolis principle as above. Each value of D_j ($j = 1, \dots, m$) is ascribed the proportion $\langle p_j \rangle$ obtained as the average over these sequences.

This "annealing" cycle was performed five times to get five distributions of the diffusion coefficient, each at its own temperature (T_0 is fluctuating) because each cycle uses a different random number sequence to produce the sequences of p_j . The final spectrum, $(D_p \langle p_j \rangle, j = 1, \dots, m)$, is the average of them and the standard deviation attached to each $\langle p_j \rangle$ was also obtained from them. This spectrum characterizes the diffusion of the labeled molecules at a given concentration within the film and for a given setup of the microscope parameters.

RESULTS AND DISCUSSION

Loading of HSA into the Film. In the first part of our study, the diffusion of proteins in the whole film section and the loading rate of proteins in the film were analyzed. Solutions of HSA^{FITC} at 3 and 10 $\mu\text{g/mL}$ have been deposited on top of (PLL/HA)₂₄-PLL films for 30 min. After rinsing with pure buffer, film sections were observed with confocal microscopy (Figure 1). A homogeneous, 7- μm thick green stripe was



Figure 1. Confocal laser scanning microscope section (x,z) images of multilayer films deposited on glass slides. (PLL/HA)₂₄-PLL multilayer films loaded with HSA^{FITC} deposited from 3 $\mu\text{g/mL}$ (a) and 10 $\mu\text{g/mL}$ solution (b). The films are visualized after rinsing with buffer solution. Thickness of the films is about 7 μm and image size is $214 \times 12 \mu\text{m}^2$. The two images were acquired using the same confocal microscope parameters.

imaged. PLL/HA films have been well characterized in several studies and it is known that the total thickness of a PLL/HA film after deposition of 24 pairs of layers is about 7 μm , in agreement with former measurements.⁹ This indicates that in the present case HSA^{FITC} diffuses through the whole film section and that the film thickness of the polymeric matrix is maintained. The larger brightness of panel b suggests that the concentration within the film is larger than in panel a.

Preliminary Observations of Films after Photobleaching. First, qualitative observations were performed to determine if proteins in the films appeared mobile over experimentally acceptable observation times. To this end, (PLL/HA)₂₄-PLL multilayer films were loaded with HSA^{FITC} from either a 1- or a 100- $\mu\text{g/mL}$ solution. A stripe was bleached at $t = 0$ and the evolution of the fluorescence intensity in this zone

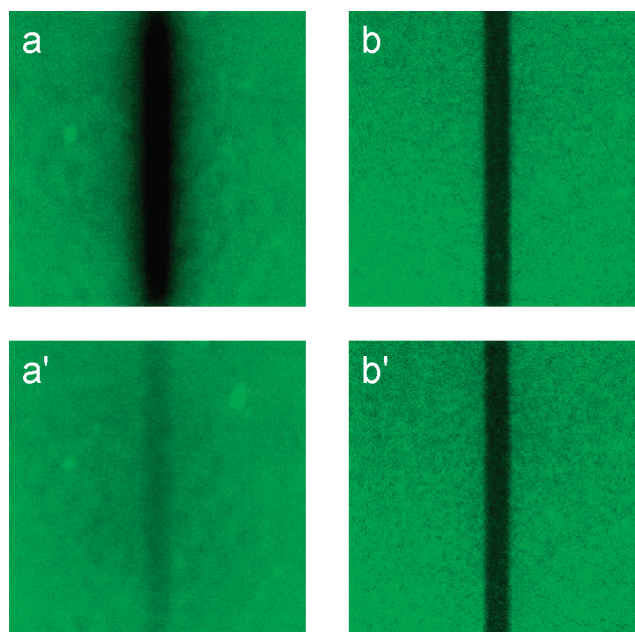


Figure 2. Representative (x,y) confocal microscope images of a (PLL/HA)₂₄-PLL-HSA^{FITC} film taken at $t = 10$ s (a and b) and $t = 600$ s (a' and b') after photobleaching. Image size is $300 \times 300 \mu\text{m}^2$. Depositions were made from 1- $\mu\text{g/mL}$ (a and a') and 100- $\mu\text{g/mL}$ (b and b') solutions of labeled proteins.

was monitored during 10 min. Figure 2 shows (x,y) images, i.e., parallel to the substrate. It appears that the recovery is nearly completed after 10 min in the low-concentration case, whereas no recovery and thus no diffusion of HSA^{FITC} is observed in the high-concentration case. This does not evidence that the molecules are immobile in Figure 2, panels b and b', but that their mobility is at least substantially reduced compared to the evolution depicted by Figure 2, panels a and a'.

To ascertain if this phenomenon is related to the loading rate of the protein in the film, we determined the amount of protein loaded in the film in our experimental conditions and extracted from FRAP data the diffusion coefficients of the protein in the film loaded at various concentrations.

Loading Rates of Labeled Human Serum Albumin in PLL/HA Films. To reveal a possible relationship between the mobility and the concentration of the protein within PLL/HA films, they have been exposed for 30 min to protein solutions of various concentrations. Protein solutions of known concentrations were used to calibrate the apparatus (UV spectrophotometer). Then, we could obtain the concentration inside the film as a function of the concentration of the solution used during the deposition (Figure 3). It may be stressed that the sole objective of this procedure was to load the film at various concentrations. The following relation can be fitted to the measured data:

$$[\text{HSA}^{\text{FITC}}]_{\text{film}} = 74800(1 - e^{-0.00317[\text{HSA}^{\text{FITC}}]_{\text{sol}}}) \quad (12)$$

where $[\text{HSA}^{\text{FITC}}]_{\text{sol}}$ and $[\text{HSA}^{\text{FITC}}]_{\text{film}}$ stand for the concentration of labeled human serum albumin in the solution and in the film, respectively. It should be noted that the film thickness stays constant at 7 μm whatever the final concentration of the protein loaded into the film. The comparison of the infrared spectrum of a PLL/HA film and the same film loaded with HSA^{FITC}, even at high protein concentration, suggests that the film loses neither water nor HA chains during the loading.

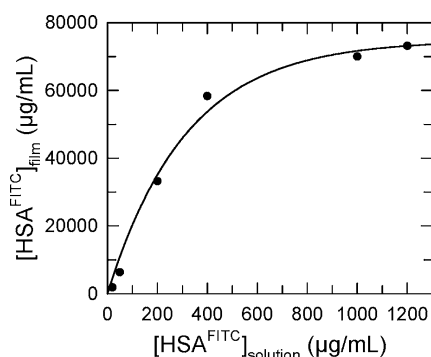


Figure 3. Relation between the concentration of HSA^{FITC} absorbed in a $(\text{PLL}/\text{HA})_{24}$ -PLL film, $[\text{HSA}^{\text{FITC}}]_{\text{film}}$ (derived from UV measurements) and its concentration $[\text{HSA}^{\text{FITC}}]_{\text{sol}}$ in the deposition solution, after 30 min deposition. The line to guide the eye corresponds to eq 12.

Figure 3 and eq 12 show that the internal concentration tends to a plateau ($\sim 75\,000\ \mu\text{g/mL}$) when the concentration of the solution used during deposition exceeds about $1000\ \mu\text{g/mL}$. The ratio of protein concentration in the film to protein concentration in solution during deposition reaches at least about 70. This result suggests that PLL/HA films have a great affinity for HSA^{FITC} or, in other words, that the internal chemical potential of these molecules is not only determined by their concentration.

As to the protein, the similarities of the infrared spectra of HSA^{FITC} in solution and in the film (see the Supporting Information) support the hypothesis that its structure remains almost unchanged upon embedding. It seems therefore that when mobility reduction is observed as the protein concentration increases, this reduction should not, or at least not primarily, be ascribed to protein denaturation which, in the present case, appears negligible. It may be stressed that during infrared measurements the HSA^{FITC} solution deposited on the film was concentrated at $1000\ \mu\text{g/mL}$. Then, as seen in Figure 3, the concentration within the film amounts to roughly $70\,000\ \mu\text{g/mL}$. So, even this 70-fold increase in concentration has only minor incidence on the infrared spectrum suggesting that even the highest HSA^{FITC} concentration in the film is moderate enough to avoid protein denaturation.

The sloping region observed for low concentrations shows that fixing the contact time (always at 30 min) and changing the solution concentration allow tuning the concentration of proteins in the film and studying the influence of this concentration on the protein mobility.

Diffusion Coefficients of Labeled Human Serum Albumin (HSA^{FITC}) for Various Loading Rates. Now, we focus on the determination of the diffusion coefficients of HSA^{FITC} in PLL/HA films with the particular aim of finding out how these coefficients dependent on the internal concentration. Three examples (0.5 , 2 , and $100\ \mu\text{g/mL}$ of HSA^{FITC} in solution) will illustrate the procedure. These concentrations are expected to lead to different spectra since observations of the FRAP images reveal a strong difference in recovery speed.

In panel a) of Figures 4–6, we show the experimental PSD (symbols) derived from the postbleach pictures, as a function of the recovery time, t (see the Computational Background section). The PSD_{exp} are computed along the 128 central lines of an image (Scheme 1) for the first three harmonics ($k = 1$ –3). They are normalized in such a way that the highest

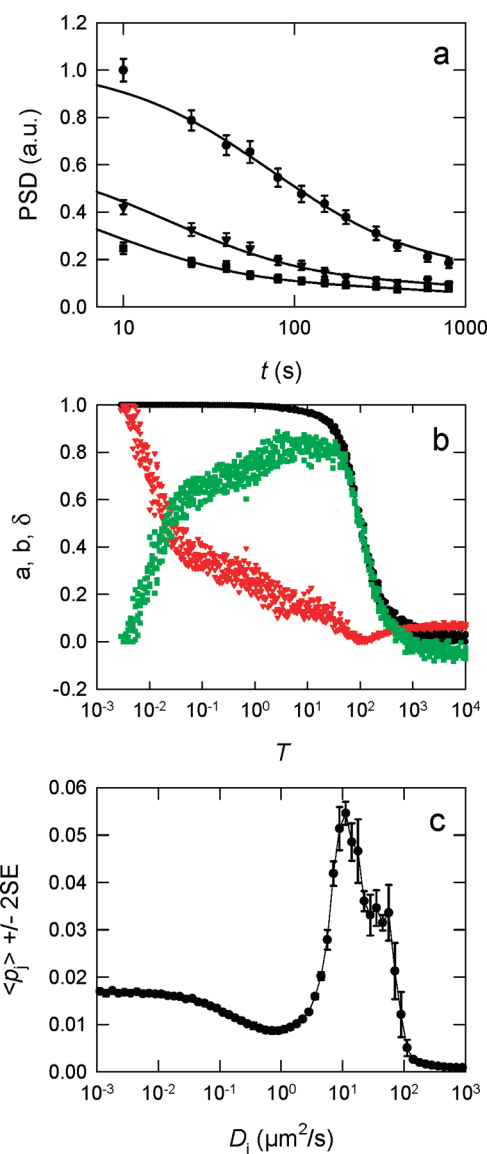


Figure 4. $(\text{PLL}/\text{HA})_{24}$ -PLL film exposed to a HSA^{FITC} solution at $0.5\ \mu\text{g/mL}$, thus of $\sim 120\ \mu\text{g/mL}$ internal concentration. (a) Values of the experimental PSD averaged over the 128 central lines of an image, for the overtones $k = 1$ (disks), 2 (triangles), and 3 (squares), derived from the fluorescence intensity as a function of the postbleach time, after subtraction of the prebleach image, using eq 5. The error bars represent ± 2 standard errors. The lines correspond to the calculated PSD (eq 6). (b) Evolution of the functions $a(T)$ (black symbols), $b(T)$ (red symbols), and $\delta(T)$ (green symbols) during the five annealing cycles. In each cycle, the maximum of $\delta(T)$ fixes the value T_0 of T at which the diffusion coefficient spectrum is derived leading to the calculated PSD shown in panel a as lines. (c) Diffusion coefficient spectrum averaged over the five simulated annealing cycles (the vertical bars are ± 2 standard errors obtained from these five independent annealing cycles).

average experimental PSD value be equal to unity (this normalization serves only to preserve the same scale in all experiments and does not alter the evaluation of the diffusion coefficients). Then, the PSD are computed using eq 6 wherein the weights p_j are optimized as described in the Computational Background section (lines in panel a) of Figures 4–6).

The evolution of the functions $a(T)$, $b(T)$ and $\delta(T)$ during the cooling process is shown in panel b) of Figures 4–6.

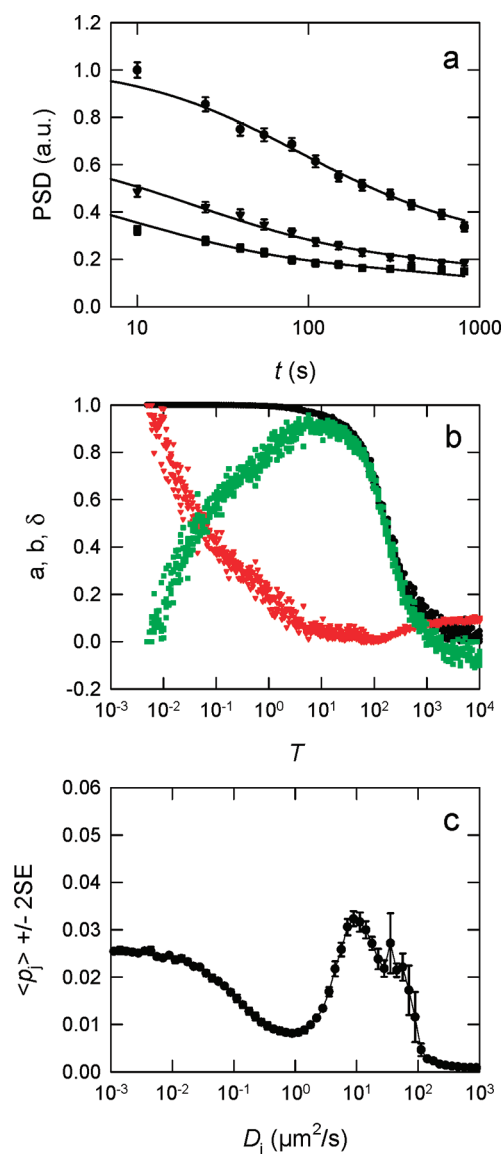


Figure 5. Same as Figure 4, except that the proteins were loaded from a solution at 2 $\mu\text{g/mL}$ (internal concentration $\sim 470 \mu\text{g/mL}$).

The maximum of $\delta(T)$ indicates the temperature, T_0 , at which the largest amount of information can be safely extracted from the available measurements. Finally, panel c) of Figures 4–6 represents the respective diffusion coefficient spectrum. In figure 4c, the main peak is located at $D_j = 10 \mu\text{m}^2/\text{s}$ and a secondary peak, though not well differentiated from the main one, might be identified at $D_j \approx 60 \mu\text{m}^2/\text{s}$. The latter one would correspond to a small proportion of labeled molecules that diffuse as in a diluted solution,²⁶ i.e., neither perturbed by neighbors nor by the polymeric environment. In contrast, the main peak corresponds to molecules with reduced mobility. Finally there are also, even at low concentration, molecules that are weakly mobile or even immobile (left wing of the spectrum: $p(D_j < 0.1 \mu\text{m}^2/\text{s}) \approx 0.32$). In Figure 5c, corresponding to $[\text{HSA}^{\text{FITC}}]_{\text{film}} = 470 \mu\text{g/mL}$, the main peak and its possible “satellite” have the same locations as for $[\text{HSA}^{\text{FITC}}]_{\text{film}} = 120 \mu\text{g/mL}$ (Figure 4c), but their intensity is reduced. Conversely, the part of slow molecules grows to 0.46. In Figure 6c, corresponding to $[\text{HSA}^{\text{FITC}}]_{\text{film}} = 20\,300 \mu\text{g/mL}$, the slow part of the tracers rises to ~ 0.71 and the peak at $D_j \geq 10 \mu\text{m}^2/\text{s}$ has disappeared. A very small bump is still visible at

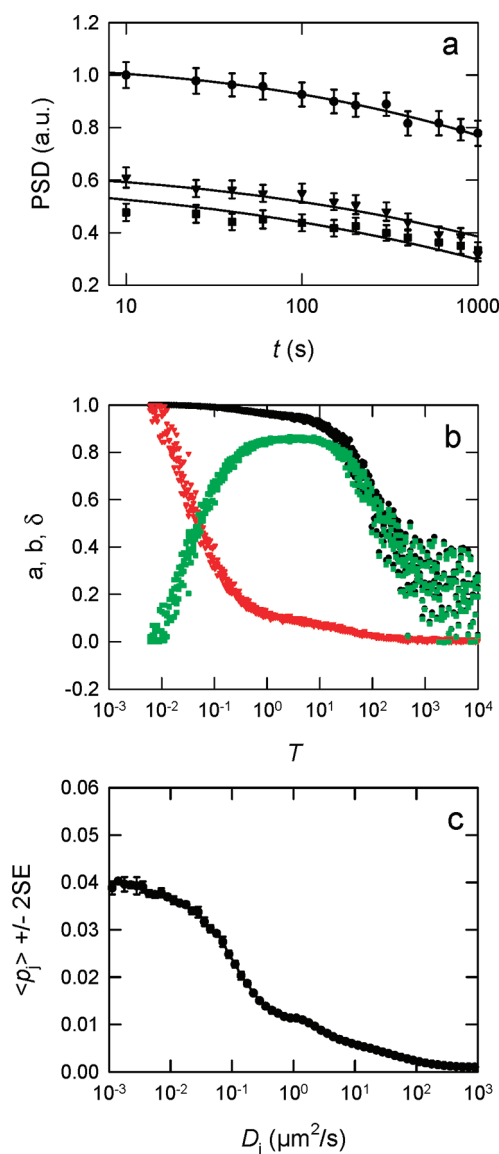


Figure 6. Same as Figure 4, except that the proteins were loaded from a solution at 100 $\mu\text{g/mL}$ (internal concentration $\sim 20\,300 \mu\text{g/mL}$).

$D_j \approx 1 \mu\text{m}^2/\text{s}$, which might be reminiscent of the rapidly moving molecules.

To strengthen the observation that the amount of slow molecules increases with the protein concentration, it is useful to sum up the proportions corresponding to all D_j smaller than a given value (e.g., $D_j < 0.1 \mu\text{m}^2/\text{s}$) and to examine how this cumulative frequency evolves with the labeled molecule concentration (Figure 7). We observe that the amount of slow molecules increases strongly over the interval 20–2000 $\mu\text{g/mL}$ of the internal concentration.

We may assume that free polycation chains decorate multicharged HSA molecules (net charge $\sim 15e$ at pH ~ 7 ,²⁵ with $e \approx -1.6 \times 10^{-19} \text{ C}$) so that the hydrodynamic radius of this combination is larger than that of the HSA molecule alone. At high enough HSA^{FITC} concentration in the film, the albumin molecules and the free polycation chains may form relatively large aggregates that diffuse slowly or even appear immobile, as may be concluded from the work of Ramasamy et al.⁴⁷ These authors mentioned aggregates whose size exceeded 100 nm that

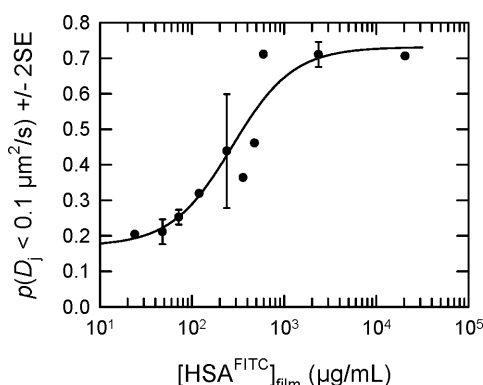


Figure 7. Cumulative proportion of “slow” molecules as a function of the protein concentration in the film obtained from the solution concentration using eq 12. The errors bars represent ± 2 standard errors. The line to guide the eye suggests the passage from the low-concentrated to the high-concentrated medium, i.e., the effect of increasing crowding on mobility.

we did not observe with confocal microscope. Nonetheless, the existence of smaller aggregates in our films cannot be visually excluded. In addition, it may be hypothesized that, as the internal concentration increases, a growing part of the albumin molecules bind at least temporarily to the positive charges of the PLL chains involved in the PLL/HA network forming the polyelectrolyte film that are not balanced out by negative charges of the hyaluronate polyanions and incompletely screened by Cl^- counterions. Furthermore, the albumin molecules themselves may form aggregates due to their own charges, as suggested by the existence of intermolecular β -sheets revealed by the infrared spectroscopy (see the Supporting Information). The probability to form such clusters is expected to increase with $[\text{HSA}^{\text{FITC}}]_{\text{film}}$. Even if there were no electrostatic interaction between HSA molecules and PLL, the meshwork constituted by the polyelectrolytes would constitute an obstacle to the diffusion of “foreign” molecules or especially clusters like does the cytoskeleton.⁴⁸ The respective roles of crowding and binding in the mobility of a protein (positively charged RNase) have been carefully investigated in solutions of positive, neutral or negative dextran at different concentrations.³⁸ It may also be mentioned that a transition from a low- to a high-concentration regime of the diffusion coefficient was already noticed in the case of aggrecan monomers and aggregates, both following the same dependence on concentration in solution.⁴⁹

It is observed that the film undergoes a crossover from a medium where the largest part of the labeled protein molecules moves “rapidly” (Figure 4c) to a crowded environment favoring both collisions and transient binding and where diffusion becomes consequently “slow” (Figure 6c). According to Figure 7, the transition to the slow diffusion regime is completed at $\sim 2000 \mu\text{g/mL}$ protein concentration in the film.

In Figure 4c, the peak extending from ~ 1 to $\sim 100 \mu\text{m}^2/\text{s}$ might be representative of the fast molecules whereas the left part of the spectrum corresponds to the slow molecules (or even apparently immobile over the observation time). To go beyond this rough subdivision into two groups of molecules, we may consider the existence of tracers with a large variety of diffusion coefficients due to diverse interaction mechanisms. Those might possibly make the overall mobility of the HSA^{FITC}

molecules inside the film to decrease with the increase of their internal concentration:

- (i) a fraction of the HSA^{FITC} molecules are isolated and diffuse in a gradually more concentrated solution ($D < 60 \mu\text{m}^2/\text{s}$), and can interact with the film matrix.
- (ii) HSA^{FITC} molecules may form dimers, trimers, ..., k -mers due to their dipolar character. At the maximum internal protein concentration ($\sim 75\,000 \mu\text{g/mL}$), the volume fraction, η , equals about 0.06 within the film. This value is below the percolation threshold $\eta_c \approx 0.34$.⁵⁰ However, two neighboring molecules are separated by a distance near the diameter of a molecule if we refer to its gyration radius $R_{\text{gyr}} = 2.74 \text{ nm}$.⁵¹ In these conditions, it may be expected that molecules collide and form aggregates through electrostatic attraction that have less mobility than the separated molecules.
- (iii) The interaction of HSA^{FITC} molecules with the free PLL chains stored inside the film, leading to complexes.⁴⁷ HSA^{FITC} -PLL complexes have probably smaller diffusion coefficients than isolated HSA molecules due to their size, but as they have a smaller global charge, they may have less electrostatic interaction with the film matrix.
- (iv) The interaction of HSA^{FITC} molecules with the PLL chains involved in the matrix of the film if the PLL charges are incompletely balanced out by the charges located on the HA chains.
- (v) The trapping of the complexes mentioned above (ii and iii) in the film meshwork for times that may have a broad distribution.

It is of course difficult to quantify the relative importance of each possibility and still more difficult to estimate the evolution with the HSA^{FITC} concentration. Each contribution leads to a proper distribution (one peak, several peaks, or a broad distribution). To attempt to show the potential existence of those peaks (or of part of them), it would be necessary to reduce progressively, down to an arbitrarily low level, the weight of the entropy in the selection of the optimum “temperature” in favor of the weight of the goodness-of-fit. This would be equivalent to departing progressively from the principle of parsimony.

We did define “slow” molecules by the arbitrary criterion $D < 0.1 \mu\text{m}^2/\text{s}$ and evaluate the corresponding cumulative proportion. This served to illustrate the consequence of increasing the internal HSA^{FITC} concentration by the evolution of a sole number. Indeed, Figure 7 suggests that the mutual interactions of the albumin molecules and the interactions between fluorescently labeled albumin molecules and either free PLL chains or the film network become increasingly important as the albumin concentration increases and induce reduction of the albumin mobility.

CONCLUSION

In this work, we have applied the FRAP method associated with spatial Fourier analysis to the evaluation of the mobility of human serum albumin, taken as a model protein, stored in a polyelectrolyte multilayer film. This film has been obtained by the alternate deposition of poly(L-lysine) and hyaluronate polyanions on a solid substrate. The film constructed in this way is relatively thick ($\sim 7 \mu\text{m}$) and highly hydrated, and did already serve as a drug reservoir.¹⁶ The simulated annealing approach, where a criterion is introduced to minimize the risk of overinterpretation of the measurements, permits the

spectrum of the diffusion coefficient to be determined, even though this spectrum may be somewhat biased because molecules diffuse already during the bleach. The present study has shown that a (PLL/HA)₂₄-PLL polyelectrolyte film has the capability to store human serum albumin at concentrations that may exceed by far those of the solutions brought into contact with the film. The FRAP method described above has revealed that the mobility of this protein within the film is largely dependent on its concentration. The crossover from the low-concentration regime to the high-concentration regime should have consequences on the release of albumin stored in the film. This point will be investigated.

■ ASSOCIATED CONTENT

■ Supporting Information

Spectrum of a (HA-PLL)₁₅ film and of a (HA-PLL)₁₅ film loaded with HSA^{FITC} obtained with Fourier transform infrared spectroscopy in the ATR mode. This material is available free of charge via the Internet at <http://pubs.acs.org>.

■ AUTHOR INFORMATION

Corresponding Author

*Phone: +33-(0)368-853258. Fax: +33-(0)368-853379. E-mail: bernard.senger@unistra.fr.

Notes

The authors declare no competing financial interest.

■ ACKNOWLEDGMENTS

C.V. acknowledges the French Ministry of Education and Research for financial support. We thank K. Benmlih for the buildup of the holders and C. Bouthier for her assistance. Confocal microscopy was carried out in Strasbourg Esplanade Cellular Imaging Facility funded by CNRS, INSERM, the University of Strasbourg and the Région Alsace.

■ REFERENCES

- (1) Decher, G. *Science* **1997**, *277*, 1232–1237.
- (2) Hiller, J.; Mendelsohn, J. D.; Rubner, M. F. *Nat. Mater.* **2002**, *1*, 59–63.
- (3) Jiang, C. Y.; Markutsya, S.; Pikus, Y.; Tsukruk, V. V. *Nat. Mater.* **2004**, *3*, 721–728.
- (4) Podsiadlo, P.; Kaushik, A. K.; Arruda, E. M.; Waas, A. M.; Shim, B. S.; Xu, J. D.; Nandivada, H.; Pumphlin, B. G.; Lahann, J.; Ramamoorthy, A.; Kotov, N. A. *Science* **2007**, *318*, 80–83.
- (5) Lee, J. S.; Cho, J.; Lee, C.; Kim, I.; Park, J.; Kim, Y. M.; Shin, H.; Lee, J.; Caruso, F. *Nat. Nanotechnol.* **2007**, *2*, 790–795.
- (6) Tang, Z. Y.; Wang, Y.; Podsiadlo, P.; Kotov, N. A. *Adv. Mater.* **2006**, *18*, 3203–3224.
- (7) Wood, K. C.; Chuang, H. F.; Batten, R. D.; Lynn, D. M.; Hammond, P. T. *Proc. Natl. Acad. Sci. U.S.A.* **2006**, *103*, 10207–10212.
- (8) Jessel, N.; Atalar, F.; Laval, P.; Mutterer, J.; Decher, G.; Schaaf, P.; Voegel, J.-C.; Ogier, J. *Adv. Mater.* **2003**, *15*, 692–695.
- (9) Picart, C.; Mutterer, J.; Richert, L.; Luo, Y.; Prestwich, G. D.; Schaaf, P.; Voegel, J.-C.; Laval, P. *Proc. Natl. Acad. Sci. U.S.A.* **2002**, *99*, 12531–12535.
- (10) Porcel, C.; Laval, P.; Ball, V.; Decher, G.; Senger, B.; Voegel, J.-C.; Schaaf, P. *Langmuir* **2006**, *22*, 4376–4383.
- (11) Nazaran, P.; Bosio, V.; Jaeger, W.; Anghel, D. F.; von Klitzing, R. *J. Phys. Chem. B* **2007**, *111*, 8572–81.
- (12) von Klitzing, R. *Phys. Chem. Chem. Phys.* **2006**, *8*, 5012–5033.
- (13) Jomaa, H. W.; Schlenoff, J. B. *Macromolecules* **2005**, *38*, 8473–8480.
- (14) Picart, C.; Mutterer, J.; Arntz, Y.; Voegel, J.-C.; Schaaf, P.; Senger, B. *Microsc. Res. Tech.* **2005**, *66*, 43–57.
- (15) Jourdainne, L.; Lécuyer, S.; Arntz, Y.; Picart, C.; Schaaf, P.; Senger, B.; Voegel, J.-C.; Laval, P.; Charitat, T. *Langmuir* **2008**, *24*, 7842–7847.
- (16) Vodouhê, C.; Le Guen, E.; Méndez Garza, J.; Francius, G.; Déjugnat, C.; Ogier, J.; Schaaf, P.; Voegel, J.-C.; Laval, P. *Biomaterials* **2006**, *27*, 4149–4156.
- (17) Wang, X.; Ji, J. *Langmuir* **2009**, *25*, 11664–11671.
- (18) Crouzier, T.; Ren, K.; Nicolas, C.; Roy, C.; Picart, C. *Small* **2009**, *5*, 598–608.
- (19) Shukla, A.; Fleming, K. E.; Chuang, H. F.; Chau, T. M.; Loose, C. R.; Stephanopoulos, G. N.; Hammond, P. T. *Biomaterials* **2010**, *31*, 2348–2357.
- (20) Shukla, A.; Avadhany, S. N.; Fang, J. C.; Hammond, P. T. *Small* **2010**, *6*, 2392–2404.
- (21) Hong, J.; Kim, B.-S.; Char, K.; Hammond, P. T. *Biomacromolecules* **2011**, *12*, 2975–2981.
- (22) He, X. M.; Carter, D. C. *Nature* **1992**, *358*, 209–215.
- (23) Szyk, L.; Schaaf, P.; Gergely, C.; Voegel, J.-C.; Tinland, B. *Langmuir* **2001**, *17*, 6248–6253.
- (24) Szyk, L.; Schwinté, P.; Voegel, J.-C.; Schaaf, P.; Tinland, B. *J. Phys. Chem. B* **2002**, *106*, 6049–6055.
- (25) Shcharbin, D.; Janicka, M.; Wasiak, M.; Palecz, B.; Przybyszewska, M.; Zaborski, M.; Bryszewska, M. *Biochim. Biophys. Acta* **2007**, *1774*, 946–951.
- (26) Berk, D. A.; Yuan, F.; Leunig, M.; Jain, R. K. *Biophys. J.* **1993**, *65*, 2428–2436.
- (27) Levitan, E. S.; Lanni, F.; Shakiryanova, D. *Nat. Protoc.* **2007**, *2*, 1117–1125.
- (28) Jönsson, P.; Jonsson, M. P.; Tegenfeldt, J. O.; Höök, F. *Biophys. J.* **2008**, *95*, 5334–5348.
- (29) Jaynes, E. T. *Phys. Rev.* **1957**, *106*, 620–630.
- (30) Sengupta, P.; Garai, K.; Balaji, J.; Periasamy, N.; Maiti, S. *Biophys. J.* **2003**, *84*, 1977–1984.
- (31) Skilling, J.; Bryan, R. K. *Mon. Not. R. Astr. Soc.* **1984**, *211*, 111–124.
- (32) Periasamy, N.; Verkman, A. S. *Biophys. J.* **1998**, *75*, 557–567.
- (33) Kirkpatrick, S.; Gelatt, C. D., Jr; Vecchi, M. P. *Science* **1983**, *220*, 671–680.
- (34) Press, W. H.; Flannery, B. P.; Teukolsky, S. A.; Vetterling, W. T. *Combinatorial minimization: Method of simulated annealing*. In *Numerical recipes in Pascal - The art of scientific computing*; Cambridge University Press: Cambridge, 1989.
- (35) Evans, R. A. *IEEE Trans. Reliab.* **1969**, *R-18*, 87–90.
- (36) Istratov, A. A.; Vyvenko, O. F. *Rev. Sci. Instrum.* **1999**, *70*, 1233–1257.
- (37) Swaminathan, R.; Periasamy, N. *Proc. Indian Acad. Sci. (Chem. Sci.)* **1996**, *108*, 39–49.
- (38) Zustiak, S. P.; Nossal, R.; Sackett, D. L. *Biophys. J.* **2011**, *101*, 255–264.
- (39) Weiss, M. *Traffic* **2004**, *5*, 662–671.
- (40) Kang, M.; Day, C. A.; Drake, K.; Kenworthy, A. K.; DiBenedetto, E. *Biophys. J.* **2009**, *97*, 1501–1511.
- (41) Saxton, M. J. *Curr. Top. Membr.* **1999**, *48*, 229–282.
- (42) Banks, D. S.; Fradin, C. *Biophys. J.* **2005**, *89*, 2960–2971.
- (43) Sullivan, K. D.; Sipprell, W. H.; Brown, E. B., Jr; Brown, E. B. *Biophys. J.* **2009**, *96*, 5082–5084.
- (44) Orlova, D. Y.; Bártová, E.; Maltsev, V. P.; Kozubek, S.; Chernyshev, A. V. *Biophys. J.* **2011**, *100*, 507–516.
- (45) Sanabria, H.; Kubota, Y.; Waxham, M. N. *Biophys. J.* **2007**, *92*, 313–322.
- (46) Metropolis, N.; Rosenbluth, A. W.; Rosenbluth, M. N.; Teller, A. H.; Teller, E. *J. Chem. Phys.* **1953**, *21*, 1087–1092.
- (47) Ramasamy, P.; El-Maghrabi, M. R.; Halada, G.; Miller, L. M.; Rafailovich, M. *Langmuir* **2007**, *23*, 2021–2029.
- (48) Klann, M. T.; Lapin, A.; Reuss, M. *Biophys. J.* **2009**, *96*, 5122–5129.

- (49) Gribbon, P.; Hardingham, T. E. *Biophys. J.* **1998**, *75*, 1032–1039.
- (50) Lorenz, C. D.; Ziff, R. M. *J. Chem. Phys.* **2001**, *114*, 3659–3661.
- (51) Kiselev, M. A.; Gryzunov, Y. A.; Dobretsov, G. E.; Komarova, M. N. *Biofizika* **2001**, *46*, 423–427.